

THESIS

SC-26196, A DELTA-6 DESATURASE INHIBITOR, NORMALIZES GLUCOSE
TOLERANCE IN OB/OB MICE

Submitted by

Melissa Anne Routh

Graduate Degree Program in Cell and Molecular Biology

In partial fulfillment of the requirements

For the Degree of Master of Science

Colorado State University

Fort Collins, Colorado

Spring 2012

Master's Committee:

Advisor: Adam J. Chicco

Gerrit Bouma
Melinda Frye
Paul Laybourn

ABSTRACT

SC-26196, A DELTA-6 DESATURASE INHIBITOR, NORMALIZES GLUCOSE TOLERANCE IN OB/OB MICE

The incidence of diabetes has reached epidemic levels worldwide, and while researchers know more about the phenomenon than ever, an effective treatment still remains elusive. Recently, chronic low-grade inflammation has been shown to play a key role in insulin resistance and diabetes. The purpose of this study was to demonstrate a role for the delta-6 desaturase (D6D) in diabetes, and furthermore to elucidate the potential mechanism by which inhibition of D6D by sc-26196 treatment could restore glucose tolerance in obese insulin resistant ob/ob mice. Treatment of 4-month-old male ob/ob mice with the selective D6D inhibitor sc-26196 (SC, 100 mg/kg/d for 4 weeks) improved response to an acute glucose challenge (1 mg/g BW i.p.), as indicated by lower peak (146% vs. 219% of fasting) and final (85% vs. 180% of fasting 2 hours-post bolus) blood glucose levels versus untreated ob/ob mice ($p < 0.01$). Increased hepatic macrophage infiltration in addition to increased phosphorylation of JNK proteins and inhibitory IRS phosphorylation in untreated ob mice was attenuated by sc-26196 treatment, which suggests that D6D inhibition improves glucose tolerance by decreasing inflammation and restoring insulin signaling by way of the IRS/PI3K pathway. This study demonstrates the

effectiveness of sc-26196 treatment for glucose intolerance in ob/ob mice and results warrant future studies for use of sc-26196 in the clinical treatment of insulin resistance and diabetes.

TABLE OF CONTENTS

ABSTRACT	ii
CHAPTER I	1
LITERATURE REVIEW	1
Increasing Incidence of Diabetes	1
Current Definition of Diabetes	1
Insulin Actions	2
Molecular Insulin Signaling	2
Inflammation and Diabetes	4
Delta-6 Desaturase and Diabetes	7
Purpose	11
CHAPTER II	12
METHODS	12
SC-26196	12
Management of Mouse Colony	12
Glucose Tolerance Tests	13
Protein Quantification by Immunoblotting	13
Tissue Preparation	13
Buffer Preparation	14

Primary and Secondary Antibodies	15
Electrophoresis Gels.....	16
Incubation Times and Temperatures	16
Visualization of Membranes.....	17
Quantification of Bands.....	17
Quantitative Real-Time PCR	17
mRNA Extraction and Purification	17
cDNA Synthesis.....	18
Real-Time Quantification	18
Primer Design	19
Serum Assays	20
Free Fatty Acids.....	20
Triglycerides	20
Insulin	21
MCP-1.....	21
Immunohistochemistry.....	21
Statistics	22
CHAPTER III.....	23
RESULTS.....	23
Mouse Weights and Food Intake.....	23
Glucose Tolerance	25
Serum Assays	29
Insulin	29

Free Fatty Acids	30
Triglycerides	30
Hepatic Insulin Signaling Immunoblots.....	31
Hepatic Macrophage Infiltration.....	32
White Adipose Tissue Macrophage Infiltration	33
Serum MCP-1	34
Hepatic Quantitative Real-Time PCR.....	35
Hepatic Delta-6 Desaturase Immunoblots.....	36
CHAPTER IV.....	37
DISCUSSION	37
CHAPTER V.....	43
SUMMARY AND CONCLUSIONS	43
REFERENCES.....	45
APPENDIX I.....	49
Modified RNA Isolation Protocol.....	50

CHAPTER I

LITERATURE REVIEW

Increasing Incidence of Diabetes

According to the 2011 National Diabetes Fact Sheet released by the Centers for Disease Control and Prevention (CDC) there are 25.8 million Americans, comprising approximately 8.3% of the United States population, currently living with diabetes. Projections indicate that prevalence of diabetes could rise as high as 33% of the US population by the year 2050 [1]. Despite medical advances, an effective and efficient treatment of diabetes currently remains elusive.

Current Definition of Diabetes

The American Diabetic Association (ADA) defines diabetes mellitus as “a group of diseases characterized by high blood glucose levels that results from defects in the body’s ability to produce and/or use insulin.” Diabetes mellitus is divided into two main subsets termed “Type 1” in which the beta cells of the pancreas are incapable of producing insulin, and “Type 2” in which the body fails to properly utilize insulin for the uptake and clearance of glucose. Both subsets result from an inability of insulin to properly signal glucose clearance. Type 2 is the most common form and accounts for 90-95% of all cases of diabetes mellitus. In Type 2 Diabetes Mellitus (T2DM), pancreatic beta cells produce the insulin necessary for

signaling; however, insulin signaling is impaired to the extent that cells are incapable of properly removing glucose from circulation. High blood glucose levels are dangerous and may lead to many complications including kidney failure, heart attack, stroke, and neuropathy among a multitude of other general health issues.

Insulin Actions

Insulin is a hormone produced in the beta cells of the pancreas that signals glucose uptake. The insulin-signaling cascade is initiated by the ingestion of glucose, which stimulates pancreatic beta cells to release insulin into the bloodstream. Once released into circulation, insulin acts primarily on muscle, liver and adipose tissues to initiate the uptake of glucose from the bloodstream and into cells. Such absorption into tissues allows the body to maintain a relatively constant blood glucose concentration even following ingestion of a large amount of glucose.

Molecular Insulin Signaling [2-4]

On a molecular level, insulin signaling begins at the insulin receptor. The insulin receptor is a receptor tyrosine kinase consisting of two extracellular alpha subunits and two transmembrane beta subunits, joined together by disulphide bonds. Insulin binding to the alpha unit of the insulin receptor causes a conformational change that initiates autophosphorylation of beta subunits. Once autophosphorylated, the tyrosine kinase domains of the beta subunits are activated and begin phosphorylating various substrates including growth factor receptor-bound protein 2 (Grb-2), and most notably a family of insulin receptor substrates including insulin receptor substrate 1 (IRS1). Several pathways diverge following phosphorylation of insulin receptor substrates. One such pathway continues

transduction from Grb-2 through the RAS/MAPK cascade and functions primarily to alter gene regulation of insulin response proteins, contributing minimally to an immediate acute response to an increase in glucose levels. Unlike the RAS/MAPK pathway, the IRS/PI3K pathway is involved in the acute response, and ultimately results in the uptake of glucose from the bloodstream and into tissues. For this reason, the IRS/PI3K pathway was been heavily researched as it offers a potential target for the treatment of insulin resistance and associated metabolic diseases. IRS-1 and IRS-2 have been heavily implicated in insulin signaling defects. Once phosphorylated by the insulin receptor, IRS proteins associate with the p85 subunit of phosphatidylinositol-3 kinase (PI3K) leading to activation of the catalytic p110 PI3K subunit, and ultimately recruitment of 3-phosphoinositide-dependent protein kinase-1 (PDK-1). PDK-1, a serine-threonine kinase, acts downstream to activate Akt, also known as Protein Kinase B (PKB), via phosphorylation at Thr308 and Ser473. Akt then phosphorylates an Akt substrate (AS160), which then causes the translocation of the glucose transporter, GLUT-4, from the cytosol of cells to the plasma membrane, allowing for the entry of glucose molecules from the bloodstream and into cells. Additionally, PDK-1 is capable of activating protein kinase C (PKC) to result in increased translocation of GLUT-4 to the plasma membrane. A brief overview of molecular insulin signaling is provided in the figure below.

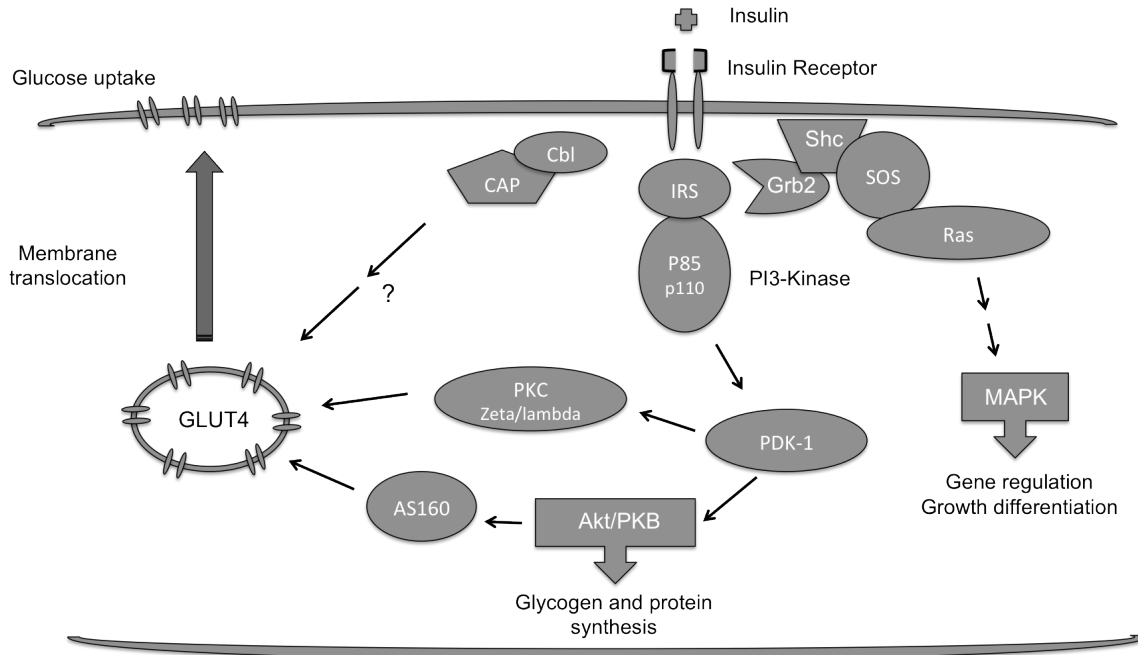


Figure 1. Molecular mechanism of insulin signaling leading to glucose uptake. Insulin binding to its receptor leads to GLUT4 translocation for glucose uptake through a signaling cascade including IRS, PI3K, Akt/PKB, and PKC proteins.

Inflammation and Diabetes

Accumulating evidence has established that obesity leading to insulin resistance and diabetes is associated with chronic low-grade inflammation and many studies have suggested that inflammation is the link between obesity, insulin resistance, and diabetes [5-7]. As in many other inflammation-associated diseases, initial inflammatory signals may ultimately become a maladaptive response that potentiates chronic inflammation, resulting in cellular damage in multiple tissues including muscle, liver and white fat.

The inflammatory response is initiated on a molecular level beginning with the cleavage of arachidonic acid from the phospholipid membrane by phospholipase A2 (PLA2) [8]. Once mobilized from the membrane by PLA2 cleavage, free AA serves

as the precursor to synthesis of strong pro-inflammatory eicosanoids including prostaglandins (PGs), thromboxanes (TXAs), leukotrienes (LTs) and hydroxyeicosatetraenoic acids (HETEs) [8]. Cyclooxygenases (COXs) are the primary enzymes responsible for the conversion of AA to PGs and TXAs, while lipoxygenases (LOs) are chiefly involved in the synthesis of LTs and HETEs from AA [9]. Eicosanoids, which are commonly referred to as the “first hormones” and are produced by every cell in the body, may ultimately be responsible for initiating and propagating the inflammatory response.

The presence of pro-inflammatory eicosanoids (PGs, TXAs, LTs, HETEs) serves as a strong indication of an inflammatory state and thus propagates the inflammatory response. In a pro-inflammatory state, immune cells initiate the release of pro-inflammatory cytokines into circulation. Cytokines are classified as lymphokines, interleukins, and chemokines, all of which bind to cell surface receptors to initiate a cellular cascade and response [10]. Several inflammatory cytokines are heavily implicated in the pathogenesis of diabetes, and include interleukin 1 β (IL-1 β), IL-6, monocyte chemoattractant protein -1 (MCP-1) and tumor necrosis factor-alpha (TNF α) [10-12]. Cytokines are extensively involved in intercellular communication and act as immunomodulators. Several studies have demonstrated the ability of TNF α , a cytokine primarily produced by fat, induces insulin resistance [13, 14]. Adiposity increases in obesity concomitantly with cytokine production as adipocytes are enlarged and damaged, leading to an excess of pro-inflammatory cytokines [6].

While interleukins and TNF α play a major role in inflammatory signaling within tissues, the primary role of MCP-1 is recruitment of macrophages to adipose and hepatic tissues [15]. Multiple studies have demonstrated an increase presence of macrophages in the adipose and hepatic tissue of obese subjects [5, 15]. Macrophage infiltration results in dysfunction by release of even more cytokines, including TNF α , IL1 β and IL6. Macrophage infiltration within tissues then further propagates the inflammatory response [6, 15-17].

Downstream of cytokine production, recent studies have established a prominent role for c-Jun amino terminal kinases (JNKs) in obesity and insulin resistance. JNK, a member of the stress-activated family of kinases, is activated via dual phosphorylation at Thr183 and Tyr185. Activation of JNK is mediated by various inflammatory cytokines including TNF α , as well as free fatty acids (FFAs) and reactive oxygen species (ROS). Once activated, JNK can phosphorylate and activate c-Jun, a proto-oncogene, which heterodimerizes with AP-1 to initiate the apoptosis signaling cascade [18]. Moreover, activated JNK has been demonstrated to inhibit IRS1 via phosphorylation at the inhibitory Ser307 site. Phosphorylation at Ser307 blocks the activating phosphorylation site, thus preventing the association of IRS1 to PI3K, which is a major initiating step in the insulin-signaling cascade.

In a study by Hirosumi et al [19], results showed that total JNK activity was significantly increased in liver, muscle and adipose tissue of various rodent models of obesity, including the ob/ob mouse. To further elucidate the importance of JNK, the group created various genetic models and demonstrated that deletion of JNK attenuated hyperglycemia and hyperinsulinemia in ob/ob mice.

As noted, the primary role of JNK in obesity and insulin resistance is inhibitory phosphorylation of IRS1 at Ser307, which interferes with proper insulin signaling and thereby proper glucose disposal from circulation. Multiple studies have established a notable role for TNF α and FFAs as strong activators of JNK proteins [19]. TNF α expression and activity, as well as serum FFA levels, are both markedly increased in obesity. This offers a mechanistic link between inflammation and insulin resistance and further suggests a central role for JNK.

Delta-6 Desaturase and Inflammation

Delta-6 desaturase (D6D), also referred to as fatty acid desaturase-2 (fads2), is the key regulator of the metabolic pathway that converts linoleic acid (18:2n6) and alpha-linolenic acid (18:3n3) to long chain polyunsaturated fatty acids (PUFAs). As illustrated in Figure 2, linoleic acid and alpha-linolenic acid compete for the initial rate-limiting enzyme D6D, resulting in the generation of arachidonic acid (20:4n-6) and docosahexaenoic acid (DHA; 22:6n-3), respectively. Through a series of steps involving various desaturating and elongating enzymes, short chain omega-3 and omega-6 fatty acids are elongated and desaturated to form such products as DHA and AA. Another notable fatty acid involved in the pathway is eicosopentaenoic acid (EPA, 20:5n3).

contributes to risk of disease by increasing the substrate for conversion to arachidonic acid and thereby the generation of potent pro-inflammatory eicosanoids [20, 21]. However, several recent studies have challenged this view, noting that dietary LA may have a neutral or beneficial effect on cardiovascular health [22, 23]; thus the subject remains highly controversial [24, 25]. Furthermore, studies examining the effect of dietary omega-6 PUFAs on insulin sensitivity are similarly equivocal [26-28]. Epidemiological studies have demonstrated strong positive correlations between serum PUFA precursor/product ratios reflective of systemic D6D activity (e.g. AA/LA) with HOMA-IR [29], BMI [29, 30], childhood obesity [31, 32], impaired fasting glucose [33], incidence of type 2 diabetes [34, 35], and the development of metabolic syndrome [36-39]. Collectively, these studies suggest a notable role for D6D in insulin resistance and diabetes.

Mechanisms responsible for increased D6D activity have not been thoroughly examined; however, D6D expression has been shown to be upregulated experimentally by hyperinsulinemia [40]. As hyperinsulinemia is a hallmark of obesity and insulin resistance, increased D6D is expected in markedly obese subjects.

D6D may be implicated in the pathogenesis of insulin resistance leading to diabetes via inflammatory modulation. As previously demonstrated, D6D is the rate-limiting enzyme involved in the production of highly unsaturated fatty acids, most notably AA. Theoretically, inhibition of D6D would result in decreased levels of AA, which would decrease the substrate necessary for eicosanoid production. Subsequently, with reduced pro-inflammatory eicosanoids, inflammatory signaling would be lessened. Diminished pro-inflammatory cytokine production would reduce

the activation of JNK. Decreasing activated JNK proteins may prevent inhibitory phosphorylation of IRS, attenuating the repression of the insulin-signaling cascade by allowing for proper actions of PI3K, Akt and GLUT4. With intact insulin transduction, glucose could be properly transported from the bloodstream and into tissues. Inhibition of D6D may thereby partially resolve glucose intolerance due to insulin resistance as illustrated in Figure 3.

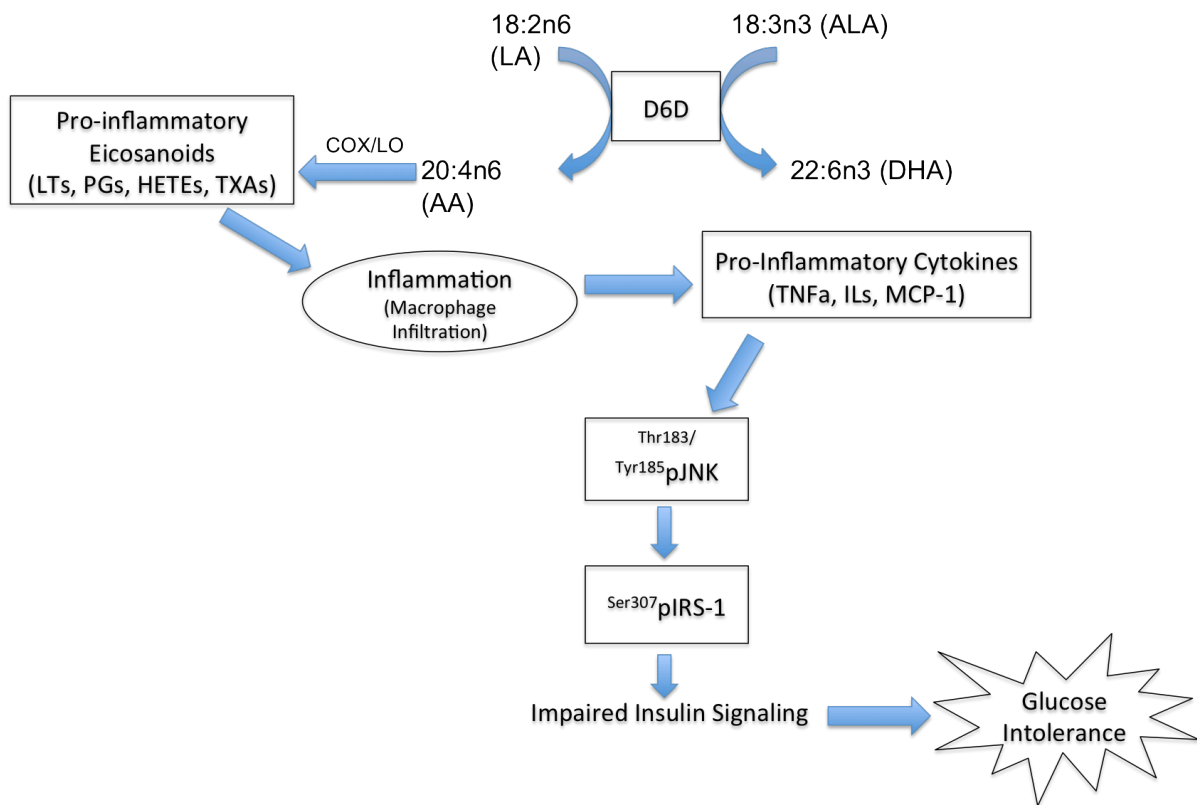


Figure 3. Proposed mechanism of D6D action in glucose intolerance. Increased D6D activity leads to increased eicosanoid production by increasing the available AA substrate. Elevated eicosanoid levels signal inflammation and macrophage infiltration leading to increased production of inflammatory cytokines that activate JNK proteins. Activated JNK inhibits IRS proteins leading to impaired insulin signaling and glucose intolerance.

Purpose

The aim of this study was to demonstrate the potential role for D6D activity in the pathogenesis of diabetes, and further to elucidate a molecular mechanism by which inhibition of D6D could attenuate glucose intolerance in the ob/ob mouse model of obesity and insulin resistance.

CHAPTER II

METHODS

SC-26196

The enzymatic D6D-specific inhibitor, sc-26196, was provided by Dr. Mark Obukowicz and is the sole property of Pfizer Corporation. The predetermined dosage of 100mg sc-26196 per kg of body weight was appropriately mixed into powdered mouse chow and fed to consc and obsc treatment groups.

Management of Mouse Colony

C57BL/6J control and ob/ob mice were purchased through Jackson Laboratories and housed in the Lab Animal Resource facility located in the Painter Building at CSU. Prior to the study, mice were fed a standard chow diet and aged to 4 months. At 4 months of age, animals were weighed, monitored, and subjected to an initial glucose tolerance test. Based on animal weights and the results of the pre-treatment glucose tolerance test, mice were sorted into one of four treatments groups: control (con; n=4), control + sc-26196 (consc; n=4), obese (ob; n=8), and obese + sc-26196 (obsc; n=8).

Mice in the con and ob groups were fed ad libitum a diet of standard powdered chow. Mice selected for the consc and obsc treatment groups were fed ad libitum powdered chow containing 100mg/kg sc-26196 based on food intake. Food

intake and body weights were monitored and recorded daily for the duration of the 4-week study. During treatment week 4, mice were subjected to post-treatment glucose tolerance test. Mice were sacrificed at the end of week 4.

Glucose Tolerance Tests

Mice were fasted for 6 hours prior to testing beginning at 7am. Each mouse was individually weighed immediately prior to glucose administration and glucose doses were calculated as a 1mg/g body weight bolus. Mouse tails were gently cleansed and swabbed and a small venous incision was made approximately 2 cm distal to the base of the tail for the collection of blood. An initial blood glucose level reading was taken prior to injection at time zero using the iStat handheld system. After the initial pre-glucose reading, mice were injected with the predetermined dose of sterile 20% (200mg/mL) dextrose solution (Hospira, Inc). Blood glucose levels were then measured and recorded every 30 minutes post-injection for 2 hours. A total of five blood glucose readings (time-points: pre-injection, 30 min, 60 min, 90 min, 120 min post injection) per mouse are reported. Results represent average blood glucose levels in mg/dL.

Protein Quantification by Immunoblotting

Tissue Preparations

Frozen tissue sections were chipped, weighed, and then immediately immersed in homogenization buffer at 1:10 w/v. Homogenization buffer consisted of

MPER lysis buffer containing a phosphatase inhibitor cocktail and was stored in aliquots at -20C until needed for use. Tissues were homogenized in buffer using glass on glass tissue grinder mortar and pestle on ice. Following homogenization, samples were flash frozen, thawed, and centrifuged for 10 minutes at 4C. After centrifugation, supernatants were transferred to new eppendorf tubes and pellets were stored at -80C. Supernatant samples containing proteins of interest were then sonicated and protein concentrations were measured by BCA assay (Thermo Sci, Catalog #23225). Following protein quantification, samples were either immediately used for immunoblotting or stored at -80C until further use.

Buffer Preparations

All buffers we prepared and diluted according to manufacturer's directions. Both stock solutions of running buffer and transfer buffer were prepared as 10X solutions and stored at room temperature prior to use. Stock solution of Running Buffer consisted of 10X Tris/Glycine/SDS Buffer (BioRad, Catalog #161-0732). Stock solution of Transfer Buffer was made with 24.7 mM Tris and 191.8 mM Glycine diluted in water to a 10X concentration.

Stock solutions were diluted and prepared as working buffers as follows. Working Running Buffer was prepared to a 1X concentration by dilution of 10X Tris/Glycine/SDS Buffer in milliQ water. Working Transfer Buffer was prepared at a 1500mL volume composed of 300mL methanol, 150mL 10X Transfer Buffer, and 1050uL milliQ water. Prior to use, working transfer buffer was chilled for

approximately 45 minutes at 4C. Wash buffer was composed of 1X TBS with 0.1% Tween-20.

Primary and Secondary Antibody Preparations

Antibodies designed to probe for proteins of interest were purchased from one of several manufacturers (AbCam, Abnova, Calbiochem, Cell Signaling ThermoScientific) and stored according to manufacturer’s instructions at 4C, -20C, or -80C. Dilutions were performed per included instructions and optimized to appropriate concentrations for detection in mouse tissue (Table 1). Primary antibodies were diluted in either 5% nonfat milk or BSA dependant on manufacturer specifications. Species-specific secondary antibodies were used at determined dilutions as noted in Table 1. Secondary antibodies were diluted in either 1% nonfat milk or BSA dependant on manufacturer instructions.

Table 1. Immunoblotting antibody ordering information and antibody dilutions.

PROTEIN	COMPANY/ CATALOGUE NUMBER	PRIMARY DILUTION	SECONDARY + DILUTION
pAkt (Ser473)	Cell Signaling #4060	1:2000 in BSA	Goat Anti-Rabbit 1:5000 in BSA
FADS2	Santa Cruz (H-40) #98480	1:200 in NFM	Goat Anti-Rabbit AP 1:2000 in NFM
F4/80	AbCam #6640	1:500 in NFM	Anti Rat-AP 1:10,000 in NFM
IκBa	Abcam #32518	1:10,000 in BSA	Goat Anti-Rabbit AP 1:5000 in BSA
IRS	Cell Signaling #2390	1:1000 in BSA	Goat Anti-Rabbit 1:5000 in BSA
pJNK (Thr183/Tyr185)	Cell Signaling #9255	1:1000 in BSA	Goat Anti-Mouse AP 1:5000 in BSA
pIRS (Ser307)	Cell Signaling #2381	1:1000 in BSA	Goat Anti-Rabbit 1:5000 in BSA

Electrophoresis Gels

2X Laemlli SDS Loading Buffer was added to diluted tissue samples containing 50ug of protein. Protein concentrations of each sample were determined by standard procedures via use of the BCA protein plate assay. Precast 4-20% Tris-HCl 26-lane gels were purchased from BioRad (Catalog #345-0034) and 15uL of sample with Laemelli loading buffer was added to each well. Additionally, 5uL of Western Protein Standards (BioRad, Catalog #161-0376) were loaded in predetermined lanes for use as a molecular weight marker.

Incubation Times and Temperatures

Gels were run in Running Buffer for approximately 45 minutes at 200V or until molecular weight markers indicated the samples had appropriately migrated to the bottom of the gel. Following gel electrophoresis, proteins were transferred onto PVDF membranes (Millipore, Catalog #ISEQ00010) in Transfer Buffer for 1 hour at 100V. After transfer, gels were stained with Coomassie Brilliant Blue and PVDF membranes were stained in Ponceau S dye to verify proper and uniform protein transfer across individual samples. Electrophoresis gels were then briefly destained and stored in acetic acid at room temperature. PVDF membranes were washed several times with milliQ water and then blocked at room temperature for 1 hour in either 5% non-fat milk or BSA according to primary antibody manufacturer's instructions. Membranes were then placed in properly diluted primary antibody (see Table 1) for overnight incubation at 4C. Following overnight incubation, membranes were washed 6 times for 5 minutes with Wash Buffer. Membranes were then placed in diluted secondary antibody for a 1-hour

incubation at room temperature. Membranes were then subjected to another 6 washes and coated with chemiluminescent substrates according to secondary conjugation for 5 minutes. HRP-conjugated secondary antibodies were incubated in West Dura Extended Duration Substrate (Thermo Sci, Catalog #34075) while AP-conjugated secondary antibodies were incubated in Immuno-Star AP Substrate (BioRad, Catalog #170-5018). Following the 5-minute incubation, membranes were prepared for visualization by UVP.

Visualization of Membranes

Membranes were visualized using a UVP Machine and exposed for several minutes until bands fluoresced at optimal levels. Alternatively, membranes used to probe for proteins with AP-conjugated secondary antibodies were also visualized using the BCIP/NBT-Blue Liquid Substrate System for membranes (Sigma, Catalog #B3804). Additionally, gels stained with Coomassie Brilliant Blue stained gels were also visualized with the UVP Software and pictures were saved for normalization of results.

Quantification of Bands

Immunoblotting results were quantified using the NIH provided software, imageJ. Results are expressed in relative units (RU) as fold changes versus control (con) mouse levels.

Quantitative Real-Time PCR

mRNA Extraction and Purification

mRNA was extracted from left ventricular samples from 4-month-old male C57Bl/6 mice and ob/ob mice using a combined modified Trizol and Qiagen protocol (Appendix I) utilizing TRI Reagent (Sigma, Catalog #T9424-100), RNeasy Mini-Kit (Qiagen, Catalog #74104), and RNase-Free DNase Set (Qiagen, Catalog #79254). All isolated RNA was purified to a 260/280 purity of >2.0 as determined by Nanodrop ND1000 Spectrophotometer. Additionally, the RNeasy MiniElute Cleanup Kit (Qiagen, Catalog #74204) was utilized to further purify samples after initial isolation, if necessary. Isolated and purified mRNA was stored at -80C.

cDNA synthesis

Extracted mRNA was thawed and diluted to a concentration of 100ng/uL and converted to cDNA by reverse transcription using the qScript cDNA Synthesis Kit (Quanta, Catalog #95047-100). A total of 20uL of cDNA was synthesized the day of intended use for Real-Time PCR quantification. Reagents were stored according to manufacturer instruction and cDNA synthesis was performed following the provided protocol.

Real-Time Quantification

Following proper cDNA synthesis, samples were prepared for Real-Time quantification by addition of SYBR Green Master Mix (Roche, Catalog #4707516001) according to manufacturer directions and stored on ice in the dark while 1.5uL of .5uM primers were loaded into each well on a 384 well LightCycler480 multiwell plate (Roche, Catalog #4729749001). Once primers were properly loaded, 8.5uL of cDNA+SYBR samples were added to each

corresponding primer well. Plates were then sealed, briefly centrifuged, and loaded into a Roche LightCycler480 Thermocycler for real-time quantification. Utilizing the provided Roche PCR template, 45 cycles of denaturing at 95°C for 10 seconds, annealing at 60°C for 30 seconds, and elongation at 72°C for 30 seconds were programmed to amplify intended primer targets. Results were collected as Cp Values and qRT-PCR data were normalized to expression of 18S rRNA, analyzed using the comparative Δ Ct method, and expressed a fold difference from WT mice. Additionally, melt-curves were examined for each data point to ensure proper primer specificity. Data are expressed as means \pm SE and compared by a students t-test with statistical significance established at $P < 0.05$.

Primer Design

Primers recognizing genes encoding proteins involved in the biosynthesis of HUFAs (*Fads2*, *Elovl5*, *Fads1*, *Elovl2*) as well as two lipogenic transcription factors known to modulate the pathway (*Ppara*, *Srebf1*) were designed using the NCBI primerBLAST program and verified for specificity by nucleotideBLAST (Table 2). Custom oligonucleotides were ordered through and manufactured by Fisher Scientific. Upon arrival, primers were tested for specificity by RT-PCR to check for a single band at the appropriate molecular weight of the intended primer target. Additionally, PCR efficiencies of each primer were tested and results yielded a PCR efficiency of 2.00 for *Srebf1*, 1.78 for *Ppara*, 1.85 for *Fads2*, 1.63 for *Fads1*, 1.40 for *Elovl5*, and 1.41 for *Elovl2*. Efficiency levels for *Fads1*, *Elovl5*, and *Elovl2* are slightly lower than the standard limit; therefore results for these three primers may yield slightly skewed results.

Table 2. Primer sequences and accession numbers for desaturases, elongases, and transcription factors involved in HUFA Biosynthesis.

Enzyme	Accession No.	Sense Sequence	Antisense Sequence
Desaturases			
<i>Fads1 (D5D)</i>	NM_146094	CCACCGACATTTCCAACAC	GGGCAGGTATTTTCAGCTTCTT
<i>Fads2 (D6D)</i>	NM_019699	TGTGTGGGTGACACAGATGA	GTTGAAGGCTGATTGGTGAA
Elongases			
<i>Elovl2</i>	NM_019423	ACGCTGGTCATCCTGTTCTT	GCCACAATTAAGTGGGCTTT
<i>Elovl5</i>	NM_134255	GGTGGCTGTTCTTCCAGATT	CCCTTCAGGTGGTCTTTCC
Transcription Factors			
<i>Ppara</i>	NM_011144	AGATTGCTGCTGACGAAATG	GGAGTGGGGAAGGTCAGTAA
<i>Srebf1</i>	NM_011480	TGACAAGCAATCAGGACCAT	TCAGCTAGGGAAAAGCCACT

Serum Assays

Free Fatty Acids

Serum free fatty acid levels were quantified using the Free Fatty Acid Quantification Kit (BioVision, Catalog #K612-100). Mouse serum was collected at the time of animal sacrifice, aliquoted, and stored at -80C. Individual serum samples were thawed, and diluted 1:10 in provided Assay Diluent to a final volume of 50uL. Free fatty acid levels were quantified using the colorimetric assay per manufacturer provided protocol and results are expressed as fold change versus control levels.

Triglycerides

Serum triglyceride levels were quantified using the Triglyceride Quantification Kit (BioVision, Catalog #K622-100). Mouse serum was collected at the time of animal sacrifice, aliquoted, and stored at -80C. Individual serum samples were thawed, and diluted 1:10 in provided Assay Diluent to a final volume of 50uL. Triglyceride levels were quantified using the colorimetric assay per manufacturer provided protocol and results are expressed as fold change versus control levels.

Insulin

Serum insulin levels were measured using the Ultra Sensitive Mouse Insulin ELISA Kit (Crystal Chem, Catalog #90080). Mouse serum was collected at the time of animal sacrifice, aliquoted, and stored at -80C. At the time of measurement, individual serum aliquots were thawed and the colorimetric assay was performed using the High Range Assay protocol per manufacturer provided instructions. Results are expressed as fold change \pm SEM versus control mouse levels.

MCP-1

Serum MCP-1 levels were quantified by Mouse CCL2 (MCP-1) ELISA Ready-SET-Go! (eBioscience, Catalog #88-7391-22). Mouse serum was collected at the time of animal sacrifice, aliquoted, and stored at -80C. At the time of measurement, individual serum aliquots were thawed, diluted 1:10 and the colorimetric assay was performed per manufacturer instruction. Results are expressed as average levels in pg/mL \pm SEM.

Immunohistochemistry

Frozen tissue sections were embedded in O.C.T. and sliced using a cryostat to be fixed on slides. Slides were prepared by Todd Bass in the Veterinary Diagnostic Lab. Elise Donovan provided the histology protocol for immunofluorescent visualization of macrophages in visceral WAT and hepatic tissue. In brief, slides were chemically de-waxed and rehydrated using xylene and ethanol. Following de-waxing, slides were blocked for 1 hour at room

temperature in block solution (5% BSA in PBS). Slides were then rinsed and 50uL of 1:100 diluted primary F4/80 antibody (AbCam, Catalog #6640) was added to each tissue section encircled by hydrophobic pen residue. Slides were incubated in primary antibody overnight at 4C. Following primary antibody incubation, slides were washed and incubated in 1:100 diluted Texas Red conjugated secondary antibody (Santa Cruz, Catalog #sc-2782) at room temperature for 1 hour in the dark. Slides were then washed and mounted with DAPI containing mounting medium (Vector, Catalog #H-1200). Fluorescence was visualized using microscopy and Metamorph software. Results are displayed as an overlay between DAPI-stained nuclei fluorescence (blue) and Texas Red conjugated secondary fluorescence indicating the presence of macrophages (red-orange).

Statistics

All results were analyzed for statistical significance using a 2-way ANOVA algorithm. Significance between groups was established at a critical value of $p < 0.05$.

CHAPTER III

RESULTS

Mouse Weights and Food Intake

Pre and Post-Treatment Weights

There were no significant differences in body weight of mice between treatment groups at the time of pre-test and terminal (post) measurements as demonstrated in Table 3 and Figure 4.

Table 3. Average body weights prior to commencement of study and following treatment at the time of animal sacrifice. Data are represented as mean \pm SEM.

	Pre (grams)	Post (grams)
Con	33.3 \pm 0.75	34.8 \pm 0.88
Consc	33.3 \pm 0.85	34.8 \pm 0.63
Ob	67.9 \pm .96	71.9 \pm 1.01
Obsc	67.4 \pm 1.08	70.6 \pm 1.16

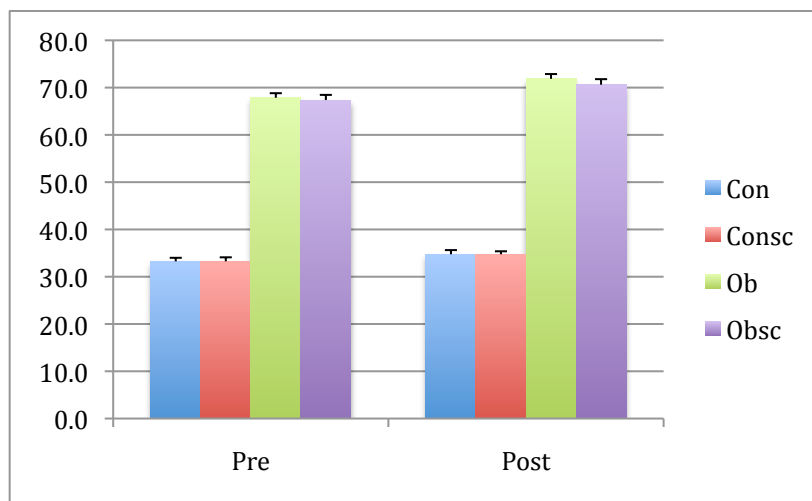


Figure 4. Average body weights prior to commencement of study and following treatment at the time of animal sacrifice. There was no notable difference within lean (con and consc) and obese (ob and obsc) groups, while the obese groups weighed substantially more than lean mice.

Food Intake

Food intake was monitored daily throughout the duration of the 4-week study, and weekly averages of presumed intake per mouse were calculated and are represented in Table 4. Though there may be a trend for increased intake in lean control mice, this is most likely due to scattering of powdered chow rather than consumption, based on higher mouse activity in the lean versus obese mice.

Table 4. Average daily food consumption calculated per mouse in grams for each week of the study. Data are represented as mean \pm SEM. Control mice food consumption appeared higher than other groups. There was no difference between ob and obsc in food consumption.

	Con	Consc	Ob	Obsc
Week 1	8.9	8.4	6.7	6.1
Week 2	8.8	7.4	7.4	7.1
Week 3	8.8	7.0	7.6	7.1
Week 4	8.8	7.9	6.9	7.0
Average	8.8 \pm 0.02	7.7 \pm 0.30	7.2 \pm 0.21	6.8 \pm 0.24

Mouse Weights Throughout Study

Over the duration of the 4-week study, lean mice (treatment groups con and consc) did not demonstrate marked weight gain, while the obese mice in both the ob and obsc treatment groups increased mass by approximately 4 grams (Table 5). There were no significant differences in body weight increases between ob and obsc mice at the time of animal sacrifice.

Table 5. Average body weight per mouse in grams for each week of the study. Data are represented as mean \pm SEM. There was no difference in body weight within lean (con and consc) and obese (ob and obsc) groups at the end of the four-week study.

	Con	Consc	Ob	Obsc
Week 1	33.5 \pm 0.22	33.9 \pm 0.63	68.7 \pm 0.72	67.4 \pm 0.26
Week 2	34.6 \pm 0.16	34.3 \pm 0.13	70.8 \pm 0.31	68.6 \pm 0.45
Week 3	34.9 \pm 0.30	35.1 \pm 0.38	71.9 \pm 0.78	70.6 \pm 0.43
Week 4	34.8 \pm 0.53	34.8 \pm 0.05	71.8 \pm 0.12	70.6 \pm 0.27
Average	34.4 \pm .32	34.5 \pm 0.27	70.8 \pm 0.75	69.3 \pm .27

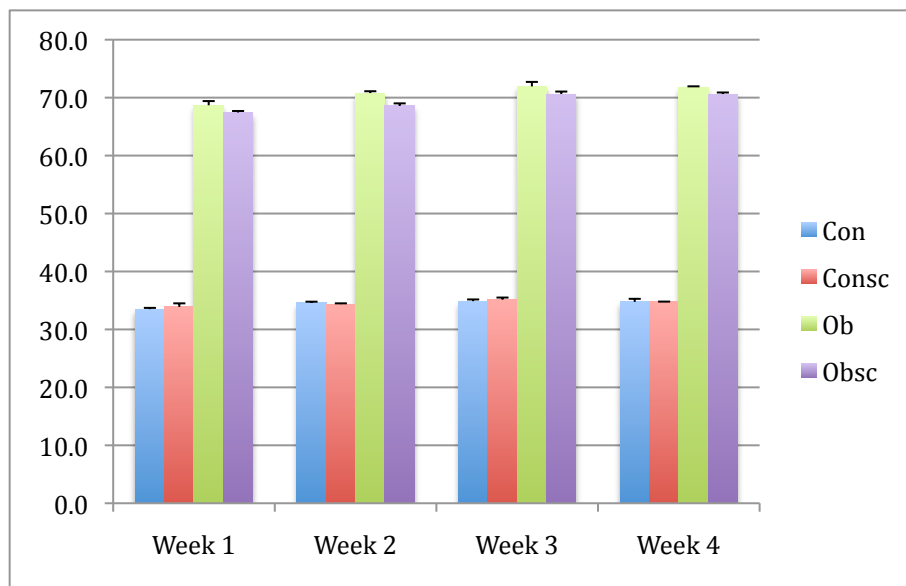


Figure 5. Average body weight per mouse in grams monitored for the duration of the study. Graphical representation of data presented in Table 5.

Glucose Tolerance

Pre-Treatment

There were no significant differences of blood glucose levels between con versus consc groups and ob versus obsc groups prior to the initiation of the study. Obese mice (ob and obsc) did demonstrate marked glucose intolerance compared to lean controls (con and consc), with blood glucose levels averaging

249 mg/dL at 2-hours post injection versus 137 mg/dL in lean controls (Table 6).

There were no differences between obsc and ob groups or between con and consc groups.

Table 6. Pre-treatment average blood glucose levels in mg/dL. Data are represented as mean \pm SEM. There was no difference in body weight within lean (con and consc) and obese (ob and obsc) groups, while the obese mice had blood sugar levels that peaked substantially higher than control mice and remained elevated 2 hours post-injection.

	Baseline	30 min	60 min	90 min	120 min
Con	147 \pm 15.3	190 \pm 19.7	167 \pm 18.1	169 \pm 14.8	148 \pm 15.3
Consc	124 \pm 4.9	168 \pm 19.5	125 \pm 22.9	139 \pm 29.5	126 \pm 33.5
Ob	173 \pm 12.0	309 \pm 35.0	300 \pm 26.6	292 \pm 18.9	253 \pm 21.9
Obsc	170 \pm 10.0	312 \pm 9.6	322 \pm 14.2	282 \pm 9.6	245 \pm 14.6

Post-Treatment

As expected, the glucose challenge resulted in significantly higher peak glucose levels (331 \pm 25.9 mg/dL vs 231 \pm 27.5 mg/dL) that remained elevated even 2 hours post injection (265 \pm 22.0 mg/dL vs 164 \pm 14.8 mg/dL) in ob mice compared to control mice (Table 7, Figure 6). Blood glucose levels 2 hours post injection were lower in sc-26196 treated ob mice compared to untreated ob mice (198 \pm 13.5 mg/dL vs 265 \pm 22.0 mg/dL, respectively; $p < .05$).

Table 7. Post-treatment average blood glucose levels in mg/dL. Data are represented as mean \pm SEM. Sc-26196 treatment resulted in blood glucose levels that returned to baseline readings 2 hours post-injection while untreated ob mouse blood glucose levels remained substantially elevated for the duration of the test.

	Baseline	30 min	60 min	90 min	120 min
Con	169 \pm 13.7	231 \pm 27.5	210 \pm 17.6	163 \pm 8.9	164 \pm 14.8
Consc	145 \pm 20.9	205 \pm 19.2	184 \pm 25.8	155 \pm 26.3	145 \pm 15.1
Ob	151 \pm 8.6	291 \pm 10.2	331 \pm 25.9	276 \pm 16.7	265 \pm 22.0
Obsc	202 \pm 19.8	321 \pm 19.1	305 \pm 15.0	259 \pm 14.4	198 \pm 13.5

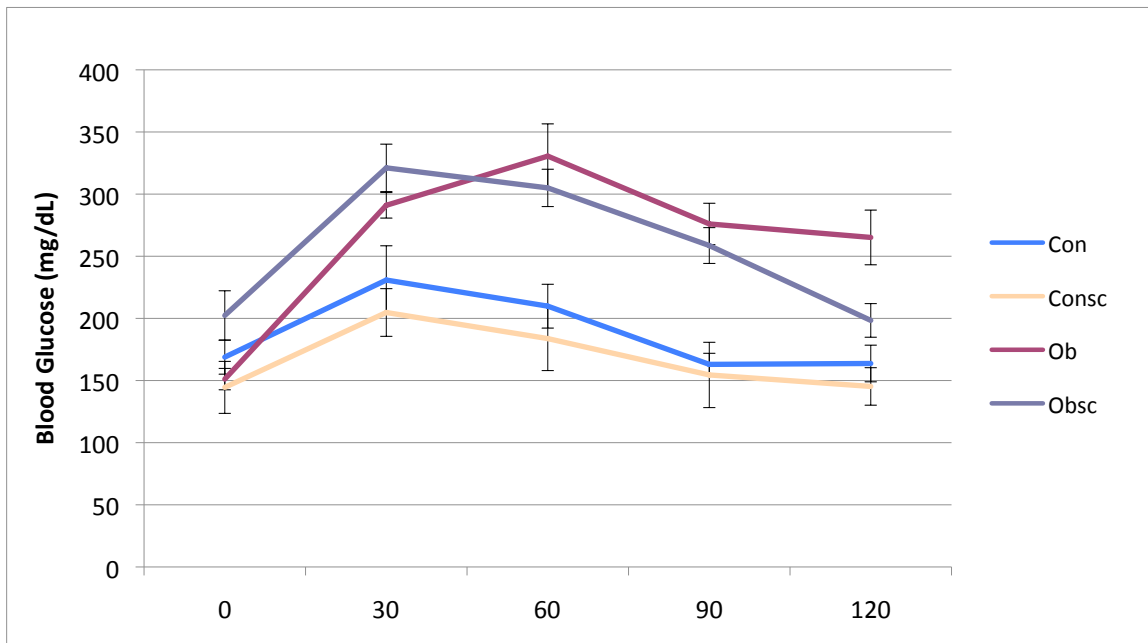


Figure 6. Post-treatment average blood glucose level in mg/dL. Visual tracing of data presented in Table 7.

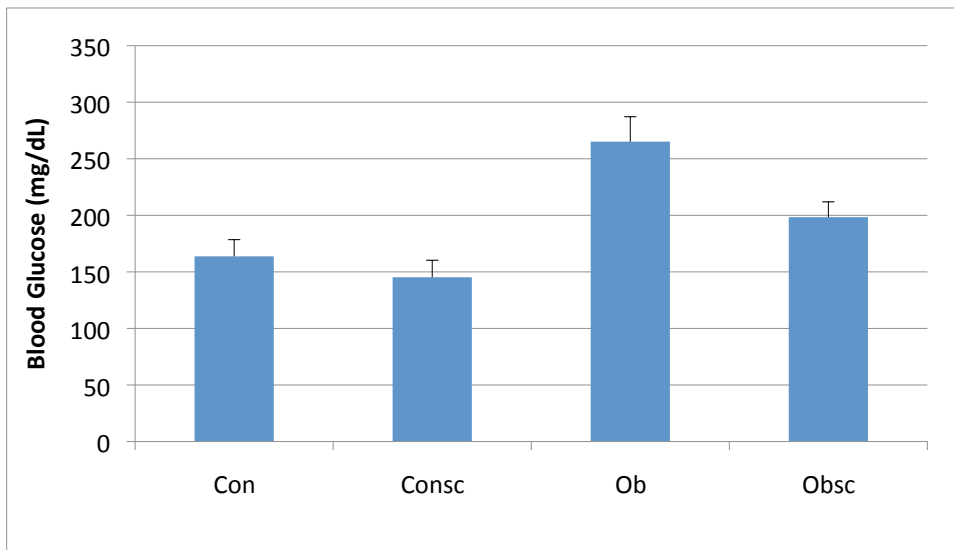


Figure 7. Post-treatment blood glucose levels at 2-hours post glucose injection. Sc-26196 treated ob mice blood glucose levels were significantly lower than untreated ob mice 2-hours post glucose challenge.

Interestingly, post-treatment fasting glucose levels at baseline were elevated in obsc mice versus ob mice (202 ± 19.8 mg/dL vs 151 ± 8.6 mg/dL). For this

reason, results were also calculated and expressed as a percentage of baseline for each time point (Table 8, Figure 8), illustrating that at 2-hours post glucose injection, only the ob mouse blood glucose levels remain significantly elevated (180 ± 19.5 mg/dL).

Table 8. Average blood glucose concentrations expressed as a percentage relative to baseline glucose levels prior to injection. Data are represented as mean \pm SEM. Con, consc, and obsc group blood glucose levels returned to baseline levels 2-hour post glucose injection, while untreated ob mouse glucose levels remained elevated.

	Baseline	30	60	90	120
Con	100	136 \pm 11.1	126 \pm 8.6	98 \pm 4.2	98 \pm 6.2
Consc	100	144 \pm 6.1	128 \pm 6.5	107 \pm 9.6	102 \pm 5.5
Ob	100	196 \pm 12.2	227 \pm 30.6	186 \pm 13.6	180 \pm 19.5
Obsc	100	166 \pm 13.9	160 \pm 16.0	134 \pm 11.5	104 \pm 11.6

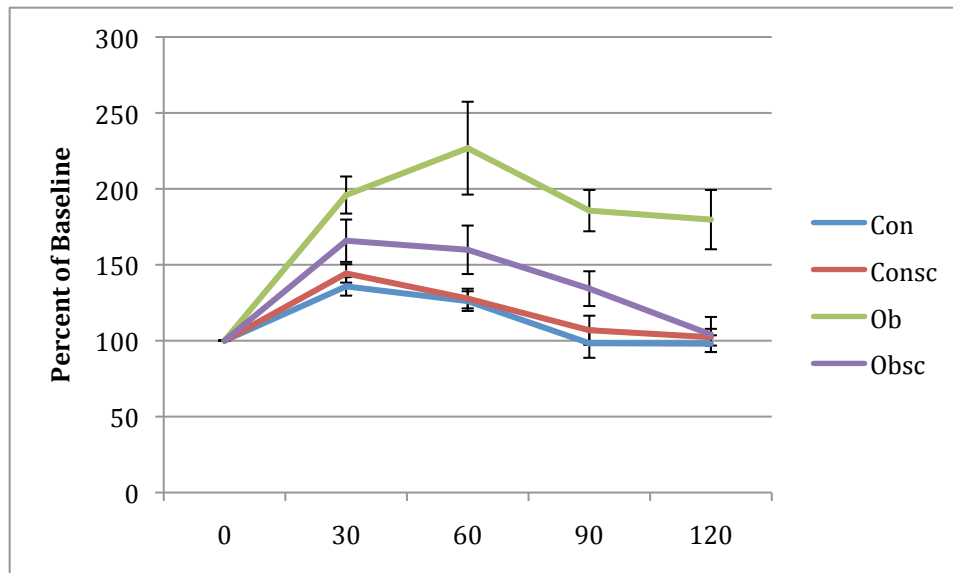
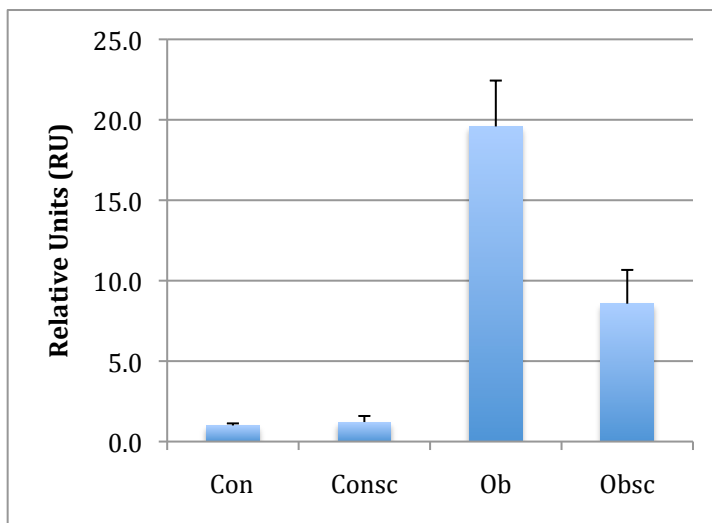


Figure 8. Average blood glucose concentrations expressed as a percentage relative to baseline glucose levels prior to injection. Graphical tracing of data presented in Table 8.

Serum Assays

Insulin

Serum insulin levels were approximately 20-fold elevated in ob mice versus lean controls ($p < 0.001$). Ob mice treated with sc-26196, had insulin levels significantly lower than untreated ob mice ($p = 0.005$).



	Insulin
Con	1 ± 0.13
Consc	1.2 ± 0.38
Ob	19.6 ± 2.85
Obsc	8.6 ± 2.10

Figure 9. Serum insulin levels expressed relative to control (con) mice levels. Data are represented as mean \pm SEM. Untreated ob mouse insulin levels were 20-fold higher than control levels, while treatment with sc-26196 significantly decreased insulin levels in ob mice.

Free Fatty Acids and Triglycerides

Serum free fatty acid and triglyceride levels were lower ($p < .05$) in ob mice versus control, and levels were further decreased in ob mice treated with sc-26196 (Figures 10, 11).

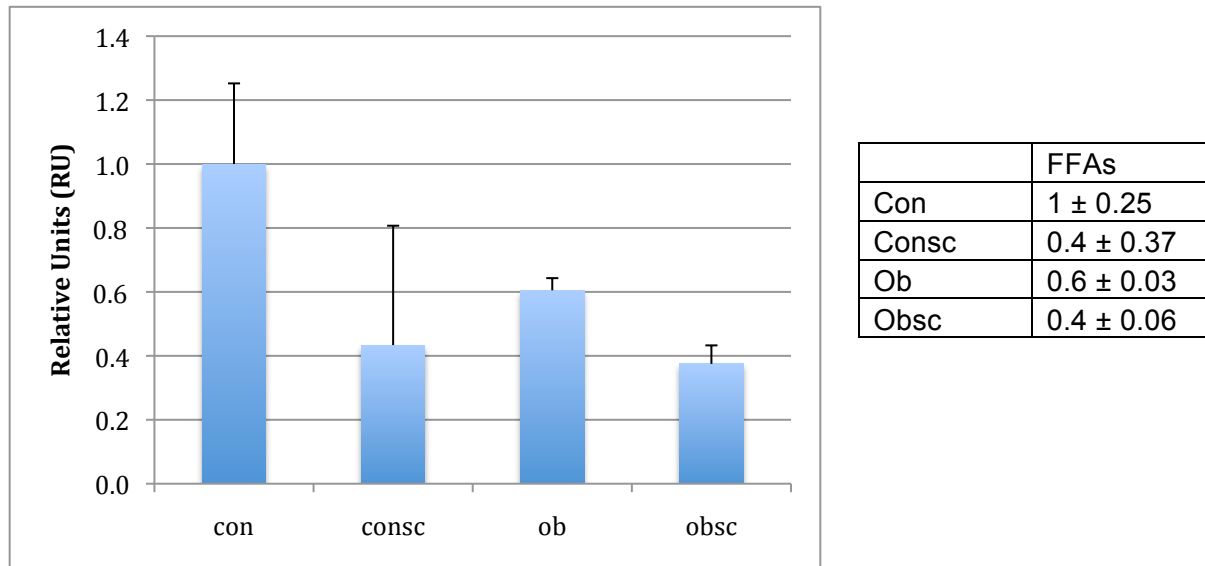


Figure 10. Serum free fatty acid levels expressed in units relative to control (con) mice levels. Data are represented as mean \pm SEM.

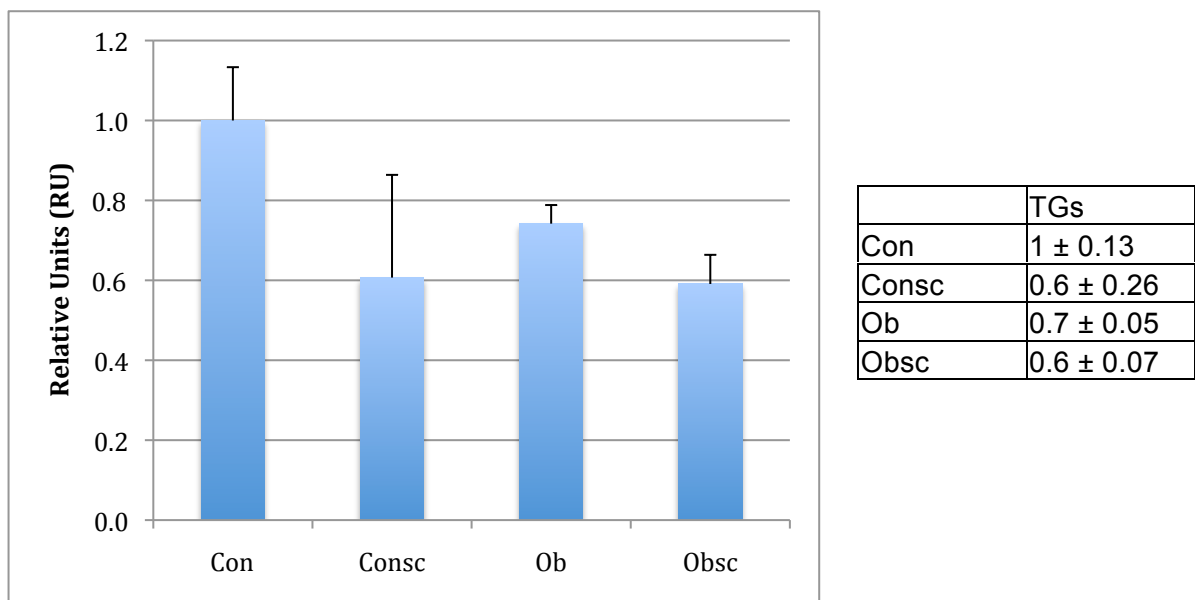


Figure 11. Serum triglyceride levels expressed in units relative to control (con) mice levels. Data are represented as mean \pm SEM.

Hepatic insulin Signaling Immunoblots

Hepatic immunoblotting results demonstrated a 3.6 ± 0.50 ($p=0.02$) fold increase in ^{S307}pIRS protein levels in ob mice that was partially attenuated by sc-26196 treatment (1.2 ± 0.41 , $p=0.03$) (Figure 12). There were no differences between IRS protein levels across treatment groups. pJNK2/3 protein levels showed a trend for increased expression between control and ob mice (1.3 ± 0.04 , $p=0.09$). Furthermore, sc-26196 treatment of ob mice decreased expression versus untreated ob mice to such an extent that was statistically insignificant compared to control group levels.

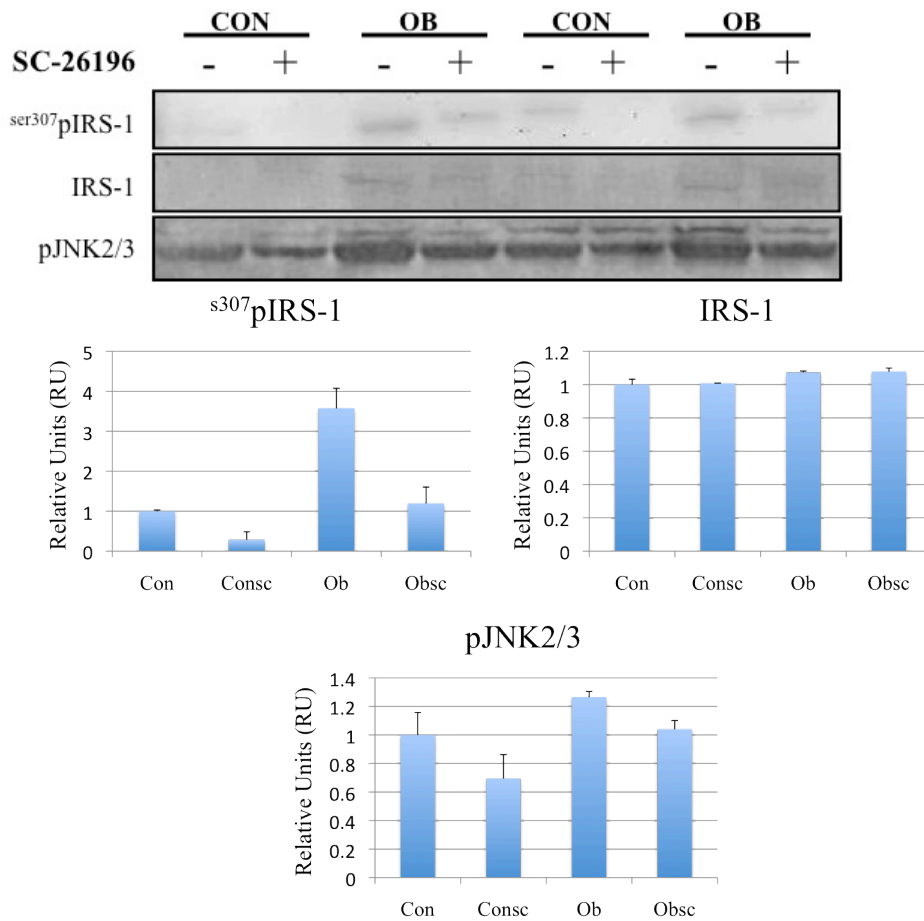
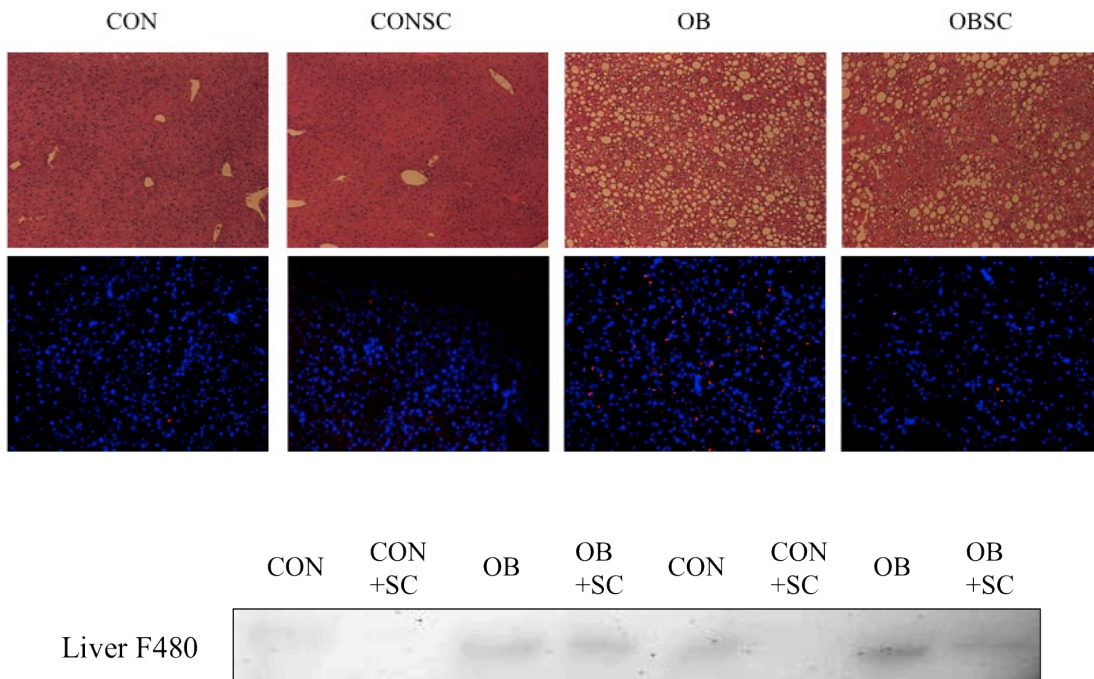


Figure 12. Immunoblotting results for ^{Ser307}pIRS-1, IRS-1, and pJNK2/3. Top: Representative western blot images. Bottom: Quantified protein levels expressed in units relative to expression in lean control (con) mice.

Hepatic Macrophage Infiltration

Examination of hepatic macrophage infiltration using the F4/80 macrophage specific antibody demonstrated increased macrophage accumulation in hepatic tissue of ob mice compared to controls as illustrated by histological analysis and immunoblotting (fold change versus control: 3.9 ± 0.82 , $p=0.04$). Sc-26196 treatment of ob mice resulted in decreased macrophage infiltration versus untreated ob mice (fold change versus control: 1.1 ± 0.56 , $p=0.05$). Interestingly, H&E stained liver histology shows increased hepatic fat droplet accumulation in obese versus control mice that was not markedly attenuated by sc-26196 treatment.



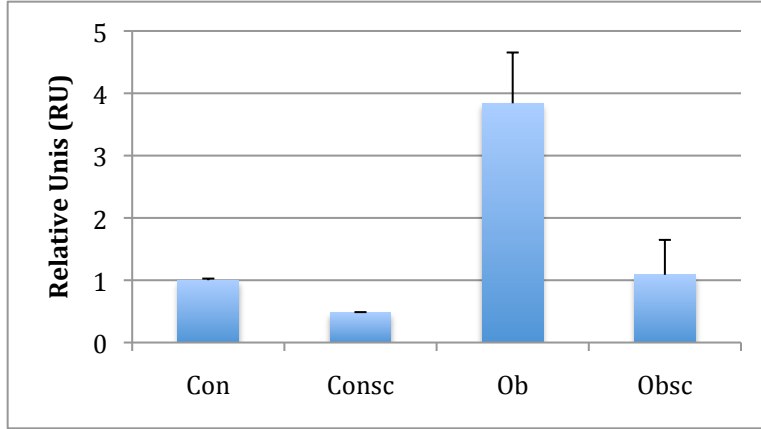
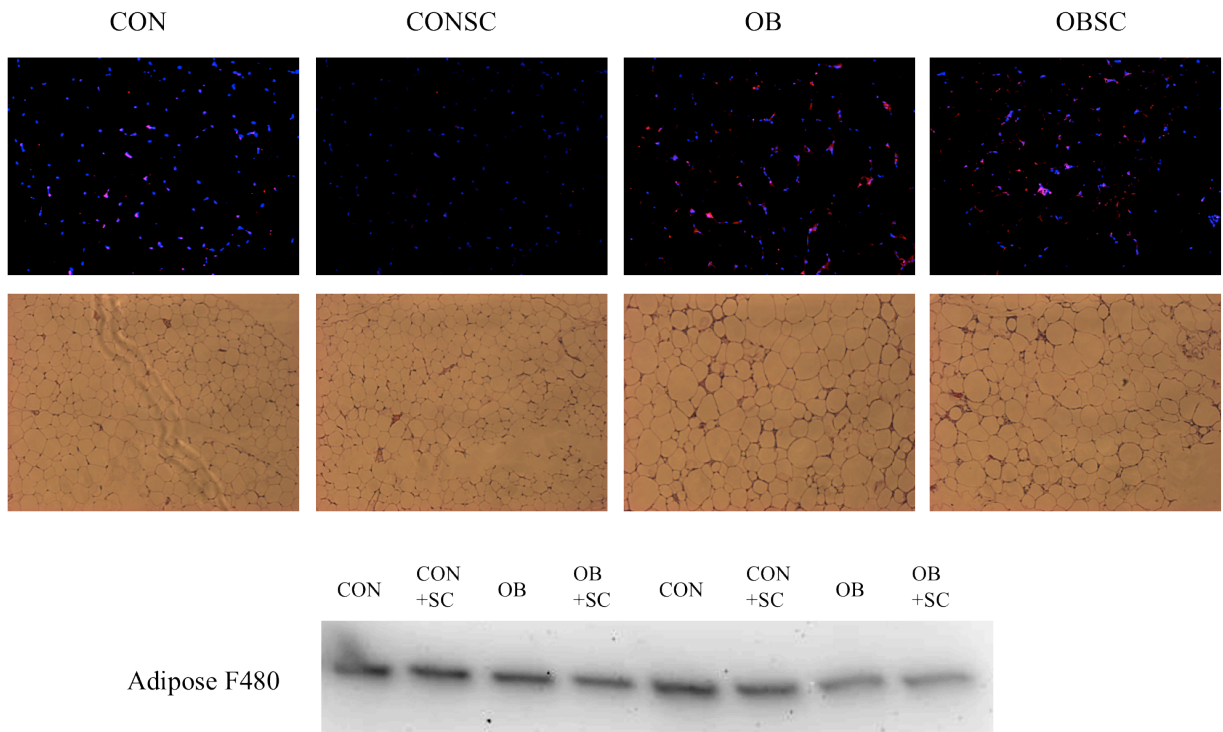


Figure 13. Hepatic macrophage infiltration. A: H&E stained liver samples. B: Immunohistochemistry analysis of the macrophage marker F4/80. C: Representative western blot for F4/80 protein content. D: Quantified F4/80 protein levels expressed in units relative to expression in lean control (con) mice.

White Adipose Tissue Macrophage Infiltration

Histological examination and immunoblotting results did not show any differences in white adipose tissue macrophage accumulation between treatment groups ($p > 0.05$).



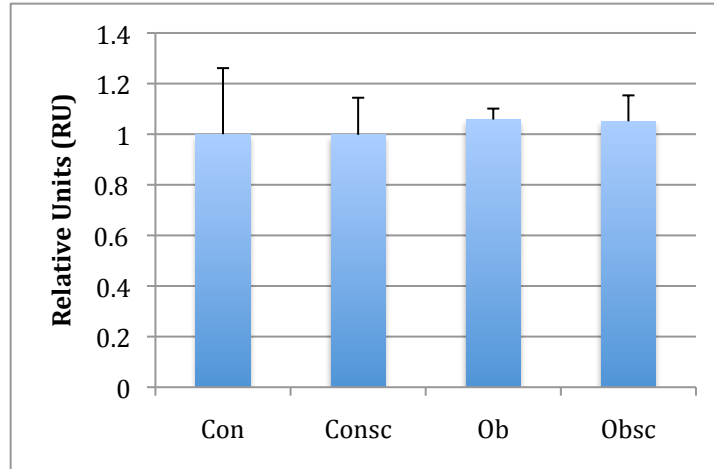
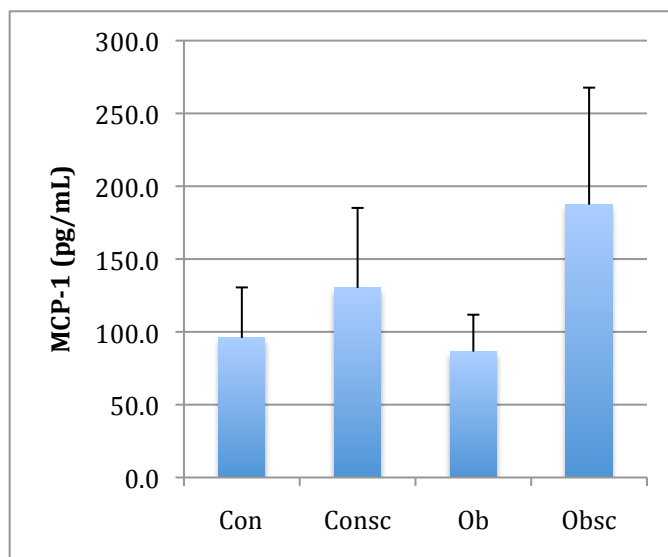


Figure 14. Hepatic macrophage infiltration. A: Immunohistochemistry analysis of the macrophage marker F4/80. B: H&E stained liver samples. C: Representative western blot for F4/80 protein content. D: Quantified F4/80 protein levels expressed in units relative to expression in lean control (con) mice.

Serum MCP-1

Serum MCP-1 levels as quantified by ELISA were not significantly different across treatment groups ($p > 0.05$); however, there was much variability among samples.



Con	95.9 ± 34.6
Consc	130.2 ± 55.0
Ob	86.4 ± 25.3
Obsc	187.4 ± 80.3

Figure 15. MCP-1 serum levels in pg/mL. Data are represented as mean ± SEM.

Hepatic Quantitative Real-Time PCR

Hepatic tissue qRT-PCR results indicated the presence of all HUFA Biosynthesis enzymes including *Fads1* and *Elovl2*, which were not detected in myocardial tissue (data not shown). Increased *Elovl5* ($p=0.02$), *Fads2* ($p<0.01$) and *Srebf1* ($p=0.03$) expression were detected in ob mice compared to controls. There were no differences in *Elovl2*, *Fads1* and *Ppara* between ob and control mice. Sc-26196 treatment of ob mice significantly decreased expression versus untreated ob mice of all genes in the HUFA Biosynthesis Pathway, including the transcription factors *Ppara* and *Srebf1* ($p<0.001$), with the exception of *Elovl5* ($p=0.10$)

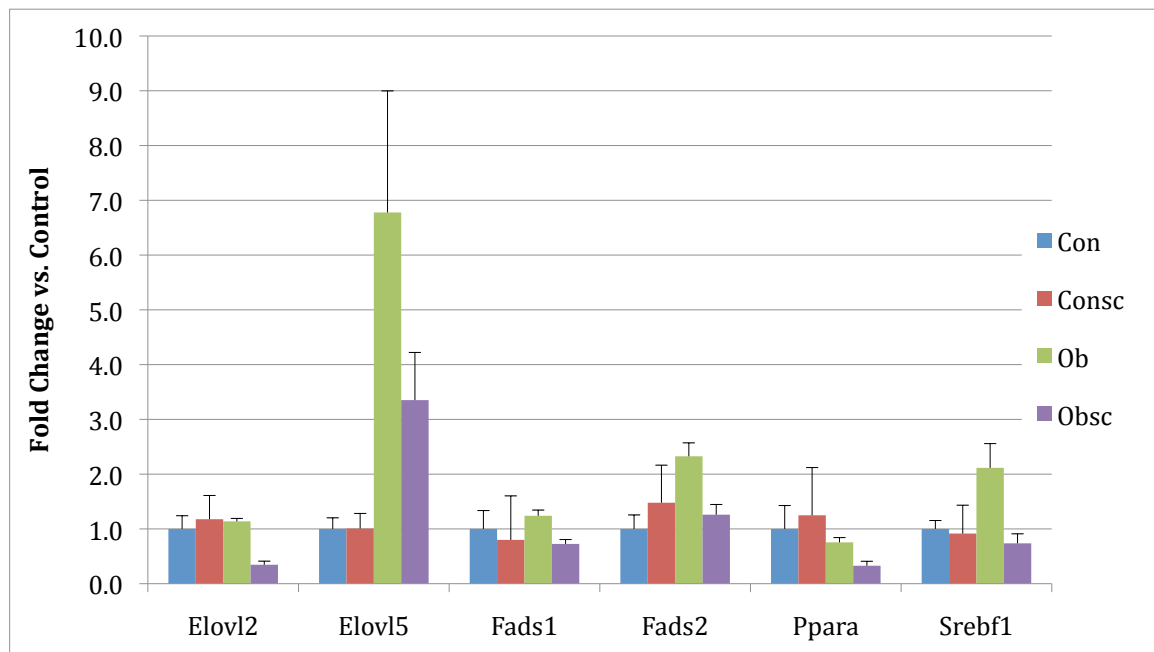


Figure 16. Quantitative Real-Time PCR results expressed as fold change versus control mice (con) expression levels. Most notably, *Fads2* mRNA levels were increased in ob mice and normalized with sc-26196 treatment.

Table 11. Quantitative Real-Time PCR results expressed as fold change versus control mice (con) expression levels. Most notably, *Fads2* mRNA levels were increased in ob mice and normalized with sc-26196 treatment.

	<i>elovl2</i>	<i>elovl5</i>	<i>d5d</i>	<i>d6d</i>	<i>ppara</i>	<i>srebf1</i>
Con	1 ± 0.24	1 ± 0.20	1 ± 0.34	1 ± 0.25	1 ± 0.43	1 ± 0.15
Consc	1.18 ± 0.43	1.01 ± 0.28	1.52 ± 0.80	1.48 ± 0.69	1.25 ± 0.87	0.92 ± 0.52
Ob	1.14 ± 0.05	6.78 ± 2.22	1.24 ± 0.11	2.33 ± 0.24	0.75 ± 0.09	2.11 ± 0.44
Obsc	.35 ± 0.07	3.35 ± 0.87	0.73 ± 0.08	1.26 ± 0.08	0.33 ± 0.08	0.74 ± 0.17

Hepatic Delta-6 Desaturase Protein

Delta-6 desaturase levels were not different across treatment groups; however, there was a trend for increased protein levels in ob versus control mice ($p=0.06$) that was partially decreased with sc-26196 treatment ($p=0.10$).

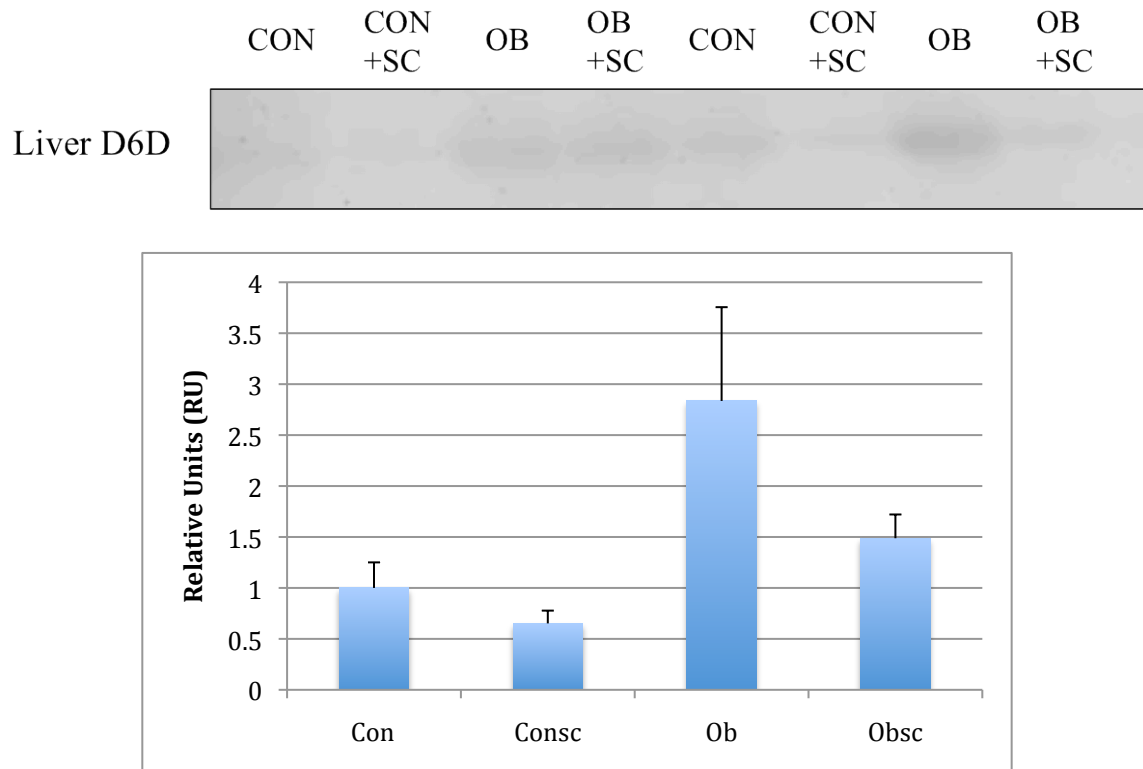


Figure 17. Hepatic D6D Protein levels. Top: Representative Western Blot for hepatic D6D. Bottom: Quantified Western Blot results expressed in relative units to control (con) mice. D6D protein expression was elevated in ob mice and sc-26196 treatment normalized D6D expression in obese mice.

CHAPTER IV

DISCUSSION

The present study aimed to demonstrate a link between the D6D inhibitor sc-26196 and the pathogenesis of diabetes, and moreover to validate a potential molecular mechanism by which inhibition of D6D could attenuate glucose intolerance in the ob/ob mouse model of obesity and insulin resistance.

Importantly, mouse weights were normalized at the initiation of the study such that there were no significant differences between the con and consc treatment groups, nor the ob and obsc groups. Based on daily food measurements throughout the duration of the study, there were no differences in the average amount of chow consumed per mouse, with the exception that the lean mice appear to have consumed slightly more chow on average versus ob mice. However, based on recorded observations, the lean mice were much more active and the apparent differences in food consumption are most likely due to playing and scattering of chow rather than consumption by the lean mice. Over the duration of the 4-week study, both lean groups gained less than 1 gram, while the obese mice gained approximately 4 grams in both the ob and obsc groups. Such measurements ensure that the effects of the study were in fact due to treatment rather than caloric restriction and weight loss in any of the testing groups.

Pre-treatment glucose tolerance tests demonstrated that ob mice were indeed unable to sufficiently handle a glucose bolus and suffered hyperglycemia at the start of the study. Post-treatment glucose tolerance test results showed significantly impaired glucose clearance in ob mice versus control that was attenuated by D6D inhibition. These results are significant in that they demonstrate a link between D6D inhibition and glucose intolerance.

Based on the results of the glucose challenge, several serum parameters were examined in an attempt to understand a mechanism by which D6D inhibition would attenuate glucose intolerance. As expected, ob mice were hyperinsulinemic with serum insulin levels approximately 20-fold higher than control mice. D6D inhibition in ob mice lowered insulin levels to nearly half that of untreated ob mice. Such marked decreases in circulating insulin may indicate that sc-treated mice are more capable of handling and clearing glucose from the circulation, so that less insulin is required to clear the same amount of glucose from the blood. Additionally, glucose levels are not as likely to increase pathologically if insulin action is effective, as demonstrated by glucose tolerance test results.

In addition to insulin levels, serum triglyceride and FFA levels were also examined. Unexpectedly, results showed that both serum triglycerides and FFA's were lower in ob mice versus controls while treatment with sc-26196 further decreased serum triglyceride and free fatty acids. Triglyceride and free fatty acid levels were expected to be elevated in obese mice in agreement with previous studies and ob/ob mouse classifications; however, the results in this study prove contrary.

To elucidate a molecular mechanism by which D6D inhibition improves glucose tolerance, key proteins involved in insulin signaling and glucose clearance were examined. As noted, serum insulin levels were drastically reduced with sc-treatment, which suggests improved insulin signaling. Since the liver is one of the primary organs involved in glucose regulation, protein levels were examined in hepatic tissue first. Notably, ^{Thr183/Tyr185}pJNK levels were increased in ob mice compared to controls and normalized by D6D inhibition. JNK proteins are commonly referred to as inflammatory-response kinases, and thus, decreased JNK protein quantity suggests decreased inflammation in sc-treated ob mice. Furthermore, downstream of JNK, results showed that inhibitory phosphorylation IRS1 at serine 307 were indeed increased in ob mice compared to controls and drastically reduced by D6D inhibition. Thus, ob mice treated with sc-26196 presumably had increased glucose tolerance due to improvements of insulin signaling by way of the IRS/PI3K pathway. These results provide a partial mechanistic link between D6D inhibition and improved glucose tolerance.

To further examine the potential that D6D was acting by way of decreasing inflammation, hepatic macrophage infiltration was examined. Histological results demonstrated that indeed there was increased accumulation of macrophages in ob versus control mice. Moreover, D6D inhibition decreased macrophage infiltration in hepatic tissue. These results were verified by immunoblotting for the macrophage marker F4/80. Macrophages are responsible for responding to and propagating cytokine release, and thus, increased accumulation of macrophages in hepatic tissue in ob mice would presumably result in increased release and presence of pro-

inflammatory cytokines including MCP-1 and TNF α . To examine this further, both cytokine markers were examined in serum by ELISA methods. MCP-1 results did not vary significantly amongst treatment groups, which suggests that perhaps MCP-1 is not the primary cytokine responsible for increased hepatic macrophage infiltration in the present study. TNF α levels were also probed in serum samples; however, ELISA methods failed to sufficiently detect the presence of TNF α in any mouse samples (data not shown). Insufficient levels of TNF α for detection may be due in part to freeze-thawed serum samples resulting in degradation. Though there was no success in measuring TNF α levels in the present study, TNF α expression was predicted to be increased in ob mice and decreased in sc-treated ob mice due to JNK phosphorylation results.

Histological examination of livers from ob mice showed large amounts of fat droplet accumulation that was not attenuated by sc-treatment. This suggests that inflammation, rather than fat accumulation, is a key contributor to glucose intolerance in hepatic tissue. Steatosis in and of itself may not be a contributing factor to the pathogenesis of glucose intolerance because sc-treated ob mice demonstrated improved glucose tolerance despite equally fatty livers as ob mice. These results support recent research demonstrating that inflammation, not steatosis, causes insulin resistance. The study showed that mice developed fatty livers without hepatic inflammation maintained normal insulin sensitivity [16]. This is not to suggest that steatosis is healthy, but rather that fatty liver in the absence of inflammation does not appear to compromise insulin sensitivity.

WAT is another tissue type commonly implicated in inflammation and the development diabetes, and so macrophage levels were examined from mouse visceral WAT. Histology results, as verified by immunoblotting, did not show significant differences in macrophage infiltration between any treatment groups. These results suggest that the mechanism for improved glucose tolerance in sc-treated ob mice does not involve reduced macrophage infiltration of WAT, and furthermore that WAT may not play as large of a role in the pathogenesis of diabetes as previously expected within the parameter of the present study.

To further establish the role of D6D in insulin resistance and glucose intolerance, mRNA expression of enzymes involved in the HUFA biosynthesis pathway were examined in hepatic tissue. Results showed a general trend for upregulation of the genes involved in the pathway in ob mice that was reversed by treatment with sc-26196. Interestingly, sc-26196 is an enzymatic inhibitor that was expected to have an effect on protein activity and not gene expression. Insulin has been demonstrated to positively regulate D6D mRNA expression; therefore, the upregulation of D6D in ob mice is likely due to increased insulin levels. Concurrently, the decreased expression of D6D in sc-treated ob mice versus untreated ob mice is likely attributable to drastically reduced circulating insulin. Additionally, there was a trend for increased D6D protein expression in ob mice that was lowered with sc-treatment, which further implicates the involvement of D6D in glucose intolerance.

As hypothesized, increased D6D expression and activity in obese insulin resistant mice leads to substantially increased production of AA derived eicosanoids, which were drastically reduced with sc-26196 treatment (data not shown).

Decreased eicosanoid production is attributable to decreased arachidonic substrate resulting from inhibiting D6D activity. Decreased levels of circulating eicosanoids results in less inflammatory stress, as demonstrated by decreased phosphorylation and activation of JNK proteins in sc-treated ob mice. Furthermore, decreased activation of JNK prevents its action as an inhibitory phosphorylator of IRS-1 at serine-307, resulting in restoration of the insulin-signaling cascade. With intact insulin signaling, cells are capable of properly extracting glucose from circulation, resulting in improved systemic glucose tolerance.

Thus, the mechanism of action of sc-26196 occurs by way of decreasing inflammatory signaling and thereby improving insulin signaling and glucose tolerance in the ob/ob mouse model of insulin resistance and obesity.

CHAPTER V

SUMMARY AND CONCLUSIONS

In recent years, an alarming and drastic increase in the incidence of diabetes has become a worldwide phenomenon. Though scientists and doctors understand the disease much more thoroughly than ever, an effective treatment remains elusive. The leptin-deficient *ob/ob* mouse has become a popular rodent model of obesity induced insulin resistance and is a powerful tool among researchers for developing effective treatments. The aim of this study was to establish a role for the enzyme delta-6 desaturase, which is the rate-limiting step in the synthesis of highly unsaturated fatty acids from essential fatty acids, in the pathogenesis of insulin resistance and diabetes. Furthermore, the present study aimed to elucidate a molecular mechanism by which inhibition of D6D by sc-26196 treatment could operate to improve glucose tolerance in *ob/ob* mice.

Methodological examination included glucose tolerance tests, serum analyses, immunoblotting, quantitative real-time PCR, immunohistochemistry, and basic histology. Treatment groups consisted of a lean control cohort of C57/BL6J mice (con), lean C57/BL6J mice treated with sc-26196 (consc), leptin-deficient *ob/ob* mice (*ob*), and finally leptin-deficient *ob/ob* mice treated with sc-26196 (*obsc*).

Treatment with the D6D inhibitor sc-26196 for four weeks restored glucose tolerance in *ob* mice, thus establishing a role for D6D in the pathogenesis of insulin

resistance and diabetes. Furthermore, ob mice exhibited increased inflammation as defined by eicosanoid production and JNK phosphorylation, accumulation of macrophages in hepatic tissue, and inhibition of key insulin-signaling proteins including IRS-1—all of which were fully or partially reversed by sc-26196 treatment. These results suggest that D6D inhibition improves glucose intolerance in ob/ob mice by decreasing systemic inflammation and restoring insulin signaling by way of the IRS/PI3K pathway.

Future Directions

Sc-26196 treatment was proven to be an effective method of increasing insulin sensitivity and restoring glucose tolerance in the ob/ob mouse model of insulin resistance and diabetes. To further ensure the molecular mechanism of action, immunoblotting and activity assays on several more of the key proteins in insulin signaling including PI3K and GLUT4 are suggested. Moreover, because D6D inhibition by sc-26196 proved to be effective in improving glucose clearance in ob/ob mice, future studies in other models of diabetes would be of great interest in developing a new treatment for diabetes in the future.

REFERENCES

1. Boyle, J.P., et al., *Projection of the year 2050 burden of diabetes in the US adult population: dynamic modeling of incidence, mortality, and prediabetes prevalence*. *Popul Health Metr*, 2010. **8**: p. 29.
2. Krook, A., H. Wallberg-Henriksson, and J.R. Zierath, *Sending the signal: molecular mechanisms regulating glucose uptake*. *Med Sci Sports Exerc*, 2004. **36**(7): p. 1212-7.
3. Pirola, L., A.M. Johnston, and E. Van Obberghen, *Modulators of insulin action and their role in insulin resistance*. *Int J Obes Relat Metab Disord*, 2003. **27 Suppl 3**: p. S61-4.
4. Pirola, L., A.M. Johnston, and E. Van Obberghen, *Modulation of insulin action*. *Diabetologia*, 2004. **47**(2): p. 170-84.
5. Heilbronn, L.K. and L.V. Campbell, *Adipose tissue macrophages, low grade inflammation and insulin resistance in human obesity*. *Curr Pharm Des*, 2008. **14**(12): p. 1225-30.
6. Shoelson, S.E., J. Lee, and A.B. Goldfine, *Inflammation and insulin resistance*. *J Clin Invest*, 2006. **116**(7): p. 1793-801.
7. Dandona, P., A. Aljada, and A. Bandyopadhyay, *Inflammation: the link between insulin resistance, obesity and diabetes*. *Trends Immunol*, 2004. **25**(1): p. 4-7.
8. Williams, K.I. and G.A. Higgs, *Eicosanoids and inflammation*. *J Pathol*, 1988. **156**(2): p. 101-10.
9. Iyer, A., et al., *Inflammatory lipid mediators in adipocyte function and obesity*. *Nat Rev Endocrinol*, 2010. **6**(2): p. 71-82.
10. Spranger, J., et al., *Inflammatory cytokines and the risk to develop type 2 diabetes: results of the prospective population-based European Prospective Investigation into Cancer and Nutrition (EPIC)-Potsdam Study*. *Diabetes*, 2003. **52**(3): p. 812-7.
11. Arner, P., *Insulin resistance in type 2 diabetes -- role of the adipokines*. *Curr Mol Med*, 2005. **5**(3): p. 333-9.

12. Vettor, R., et al., *Review article: adipocytokines and insulin resistance*. *Aliment Pharmacol Ther*, 2005. **22 Suppl 2**: p. 3-10.
13. Hotamisligil, G.S., N.S. Shargill, and B.M. Spiegelman, *Adipose expression of tumor necrosis factor-alpha: direct role in obesity-linked insulin resistance*. *Science*, 1993. **259**(5091): p. 87-91.
14. Feinstein, R., et al., *Tumor necrosis factor-alpha suppresses insulin-induced tyrosine phosphorylation of insulin receptor and its substrates*. *J Biol Chem*, 1993. **268**(35): p. 26055-8.
15. Chawla, A., K.D. Nguyen, and Y.P. Goh, *Macrophage-mediated inflammation in metabolic disease*. *Nat Rev Immunol*, 2011. **11**(11): p. 738-49.
16. de Luca, C. and J.M. Olefsky, *Inflammation and insulin resistance*. *FEBS Lett*, 2008. **582**(1): p. 97-105.
17. Samaan, M.C., *The macrophage at the intersection of immunity and metabolism in obesity*. *Diabetol Metab Syndr*, 2011. **3**(1): p. 29.
18. Bennett, B.L., Y. Satoh, and A.J. Lewis, *JNK: a new therapeutic target for diabetes*. *Curr Opin Pharmacol*, 2003. **3**(4): p. 420-5.
19. Hirosumi, J., et al., *A central role for JNK in obesity and insulin resistance*. *Nature*, 2002. **420**(6913): p. 333-6.
20. Salem, N., Jr. and R.J. Pawlosky, *Arachidonate and docosahexaenoate biosynthesis in various species and compartments in vivo*. *World Rev Nutr Diet*, 1994. **75**: p. 114-9.
21. Okuyama, H., T. Kobayashi, and S. Watanabe, *Dietary fatty acids--the N-6/N-3 balance and chronic elderly diseases. Excess linoleic acid and relative N-3 deficiency syndrome seen in Japan*. *Prog Lipid Res*, 1996. **35**(4): p. 409-57.
22. Harris, W.S., et al., *Omega-6 fatty acids and risk for cardiovascular disease: a science advisory from the American Heart Association Nutrition Subcommittee of the Council on Nutrition, Physical Activity, and Metabolism; Council on Cardiovascular Nursing; and Council on Epidemiology and Prevention*. *Circulation*, 2009. **119**(6): p. 902-7.
23. Willett, W.C., *The role of dietary n-6 fatty acids in the prevention of cardiovascular disease*. *J Cardiovasc Med (Hagerstown)*, 2007. **8 Suppl 1**: p. S42-5.
24. Ramsden, C.E., J.R. Hibbeln, and W.E. Lands, *Letter to the Editor re: Linoleic acid and coronary heart disease. Prostaglandins Leukot. Essent. Fatty Acids (2008), by W.S. Harris*. *Prostaglandins Leukot Essent Fatty Acids*, 2009. **80**(1): p. 77; author reply 77-8.

25. Ramsden, C.E., et al., *n-6 fatty acid-specific and mixed polyunsaturate dietary interventions have different effects on CHD risk: a meta-analysis of randomised controlled trials*. Br J Nutr, 2010. **104**(11): p. 1586-600.
26. Jucker, B.M., et al., *Differential effects of safflower oil versus fish oil feeding on insulin-stimulated glycogen synthesis, glycolysis, and pyruvate dehydrogenase flux in skeletal muscle: a ¹³C nuclear magnetic resonance study*. Diabetes, 1999. **48**(1): p. 134-40.
27. Brady, L.M., et al., *Increased n-6 polyunsaturated fatty acids do not attenuate the effects of long-chain n-3 polyunsaturated fatty acids on insulin sensitivity or triacylglycerol reduction in Indian Asians*. Am J Clin Nutr, 2004. **79**(6): p. 983-91.
28. Asp, M.L., et al., *Time-dependent effects of safflower oil to improve glycemia, inflammation and blood lipids in obese, post-menopausal women with type 2 diabetes: a randomized, double-masked, crossover study*. Clin Nutr, 2011. **30**(4): p. 443-9.
29. Warensjo, E., et al., *Associations between estimated fatty acid desaturase activities in serum lipids and adipose tissue in humans: links to obesity and insulin resistance*. Lipids Health Dis, 2009. **8**: p. 37.
30. Park, H., et al., *The fatty acid composition of plasma cholesteryl esters and estimated desaturase activities in patients with nonalcoholic fatty liver disease and the effect of long-term ezetimibe therapy on these levels*. Clin Chim Acta. **411**(21-22): p. 1735-40.
31. Decsi, T., D. Molnar, and B. Koletzko, *Long-chain polyunsaturated fatty acids in plasma lipids of obese children*. Lipids, 1996. **31**(3): p. 305-11.
32. Decsi, T., D. Molnar, and B. Koletzko, *The effect of under- and overnutrition on essential fatty acid metabolism in childhood*. Eur J Clin Nutr, 1998. **52**(8): p. 541-8.
33. Laaksonen, D.E., et al., *Serum fatty acid composition predicts development of impaired fasting glycaemia and diabetes in middle-aged men*. Diabet Med, 2002. **19**(6): p. 456-64.
34. Hodge, A.M., et al., *Plasma phospholipid and dietary fatty acids as predictors of type 2 diabetes: interpreting the role of linoleic acid*. Am J Clin Nutr, 2007. **86**(1): p. 189-97.
35. Kroger, J., et al., *Erythrocyte membrane phospholipid fatty acids, desaturase activity, and dietary fatty acids in relation to risk of type 2 diabetes in the European Prospective Investigation into Cancer and Nutrition (EPIC)-Potsdam Study*. Am J Clin Nutr. **93**(1): p. 127-42.

36. Decsi, T., et al., *Polyunsaturated fatty acids in plasma lipids of obese children with and without metabolic cardiovascular syndrome*. *Lipids*, 2000. **35**(11): p. 1179-84.
37. Kawashima, A., et al., *Plasma fatty acid composition, estimated desaturase activities, and intakes of energy and nutrient in Japanese men with abdominal obesity or metabolic syndrome*. *J Nutr Sci Vitaminol (Tokyo)*, 2009. **55**(5): p. 400-6.
38. Vessby, B., *Dietary fat, fatty acid composition in plasma and the metabolic syndrome*. *Curr Opin Lipidol*, 2003. **14**(1): p. 15-9.
39. Warensjo, E., U. Riserus, and B. Vessby, *Fatty acid composition of serum lipids predicts the development of the metabolic syndrome in men*. *Diabetologia*, 2005. **48**(10): p. 1999-2005.
40. Brenner, R.R., *Hormonal modulation of delta6 and delta5 desaturases: case of diabetes*. *Prostaglandins Leukot Essent Fatty Acids*, 2003. **68**(2): p. 151-62.

APPENDIX I

Modified mRNA Isolation Protocol

Trizol and Qiagen RNeasy Kit

1. Add tissue to 1mL Trizol.
2. Homogenize tissue.
3. Add 200uL Chloroform and vortex 15s. Centrifuge at max for 15m.
4. Transfer ~500uL top aqueous phase to new tube.
5. Add 500uL Buffer RLT.
6. Add 1mL 70% ethanol and mix by inverting.
7. Add all solution to RNeasy column 700uL at a time and spin through 15s at 10,000 rpm.
8. Add 700uL Buffer RW1 and spin through columns 15s at 10,000rpm. Discard flow through.
9. Thaw aliquot tubes of DNase needed. Add 350uL Buffer RDD to each aliquot tube.
10. Add 80uL DNase+Buffer RDD to each column. Incubate at RT for 15m.
11. Wash with 700uL Buffer RW1 and spin through columns 15s at 10,000rpm. Discard flow through.
12. Transfer to new 2mL collection tube.
13. Wash with 500uL Buffer RPE and spin through 2m at 10,000rpm. Discard flow through.
14. Spin columns dry 1m at full speed.
15. Allow to air dry and place column into clean 1.5mL Eppendorf tube from kit.
16. Add 30uL of RNase free water from kit and allow to absorb for 1min.
17. Elute by centrifuging 1m at 10,000rpm.
18. Pass elute through column again to improve RNA yield.
19. Quantify using Nanodrop.